

# Shedding Light on the Nature of Photoinduced States Formed in a Hydrogen Generating Supramolecular RuPt Photocatalyst by Ultrafast Spectroscopy

## Supporting Information

Annemarie Huijser<sup>a‡</sup>, Qing Pan<sup>a%</sup>, David van Duinen<sup>a§</sup>, Mads G. Laursen<sup>b</sup>, Amal El Nahhas<sup>c</sup>, Pavel Chabera<sup>c</sup>, Leon Freitag<sup>d</sup>, Leticia González<sup>d</sup>, Qingyu Kong<sup>e§</sup>, Xiaoyi Zhang<sup>e</sup>, Kristoffer Haldrup<sup>b</sup>, Wesley R. Browne<sup>f</sup>, Grigory Smolentsev<sup>g,h</sup> and Jens Uhlig<sup>\*c‡</sup>

<sup>a</sup> University of Twente, MESA+ Institute, Optical Sciences and PhotoCatalytic Synthesis groups, PO Box 217, 7500 AE Enschede, The Netherlands.

<sup>b</sup> Technical University of Denmark, Department of Physics, 2800 Kgs Lyngby, Denmark.

<sup>c</sup> Lund University, Department of Chemical Physics, Getingevägen 60, Lund 22100, Sweden.

<sup>d</sup> Institute of Theoretical Chemistry, Faculty of Chemistry, University of Vienna, Währinger Str. 17, 1090 Vienna, Austria.

<sup>e</sup> Argonne National Laboratory, X-ray Sciences Division, Illinois 60439, United States.

<sup>f</sup> University of Groningen, Stratingh Institute for Chemistry, Molecular Inorganic Chemistry group, 9747 AG Groningen, The Netherlands.

<sup>g</sup> Paul Scherrer Institute, Villigen 5232, Switzerland.

<sup>h</sup> Smart Materials International Research Center, Southern Federal University of Russia, Rostov-on-Don, 344090, Russian Federation.

## Contents

- 1) Models tested for difference XANES and EXAFS structure characterization
- 2) FEFF parameters used for calculation of models
- 3) Photoluminescence at various excitation wavelengths
- 4) Differential absorbance spectra at reduction conditions
- 5) Transient absorption spectra at various excitation wavelengths
- 6) Time-Dependent Density Functional Theory calculations of optical transitions
- 7) Comparison of white line intensity of modeled and measured XANES

### *1) Models tested for difference XANES and EXAFS structure characterization*

These structures and structural modifications were tested to model the difference XANES spectrum. The arrows indicate the “movements” that we applied to atoms/atomic groups (typically in 10 steps in rotation/translation in a reasonable range) to create different structures. In addition to these movements each group was moved to an interatomic distance of 10 Å, effectively removing it from the Pt. At each of these structural points a matrix of electron occupation (Fermi level parameter in FEFF) and the chemical shift was calculated and compared to the measured spectrum. The structures in cells marked with grey and some selected movements of were also used as steady state structural input models into the EXAFS analysis. The fitting was performed with the routines provided by Artemis and the bond distances reported in the manuscript.

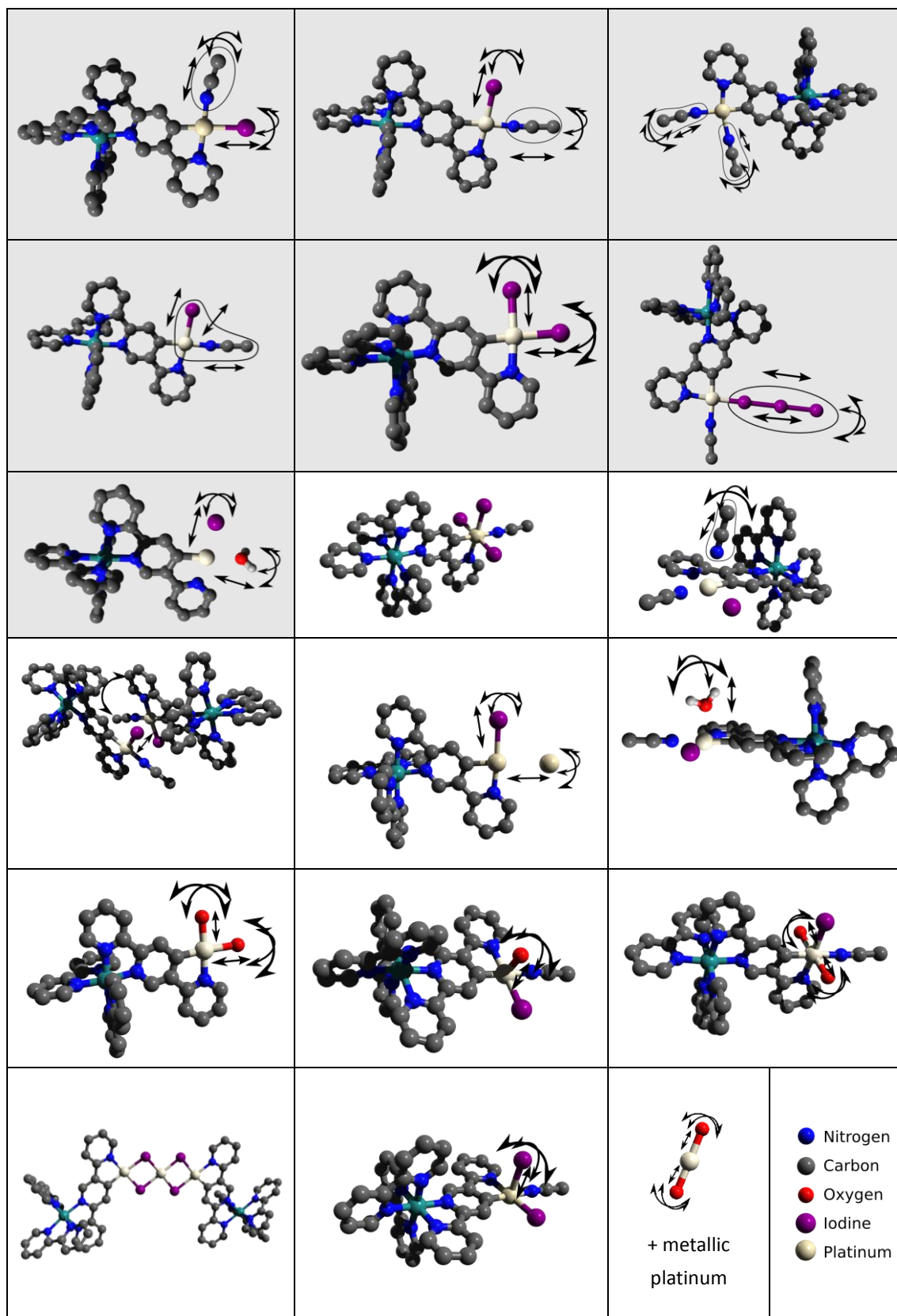


**Figure S1.** Molecular modulations used for calculating the EXAFS (grey) and XANES (all) spectra. Arrows indicate the directions/angles that were modulated.

## 2) FEFF parameters used for calculation of models

Ground state parameter:

TITLE RuPt

CONTROL 1 1 1 1 1 1

EDGE L3

CHWIDTH 4.2

PRINT 2 2 0 1 0 1

EGRID

e\_grid -26.917560 173.082440 0.5

S02 0.9

EXCHANGE 0 -0.9 0.0 2

SCF 8.0 1 30 0.2 10

COREHOLE RPA

FMS 8.0 0

XANES 7 0.05 0.1

Reduced state (RS) parameter:

changed Fermi level in EXCHANGE card by -1.0 eV (to -1.9 eV)  
chemical shift of -0.2 eV.

Oxidized state (HP) parameter:

changed Fermi level in EXCHANGE card by +1.9 eV (to +1.0 eV),  
chemical shift of +2.5 eV.

### 3) Photoluminescence at various excitation wavelengths

Here we show steady state absorption and emission measurements of RuPt and Ru[bpy]<sub>3</sub><sup>2+</sup> in solution. The unsubstituted Ru[bpy]<sub>3</sub><sup>2+</sup> dye has been used as reference to account for potential variations in excitation intensity. Excitation was provided by a Xenon lamp (75 W) coupled to a Zolix (150) Omni monochromator with slits set to give a bandwidth of 10 nm (FWHM). The sample was held in a QNW-qmode temperature controlled cuvette holder and emission collected at 90° with a 50 micron round to line fibre bundle (Thorlabs) and feed into a Andor Technology Shamrock163 spectrograph equipped with a 500 nm blaze (150 l/mm) grating and Andor Technology CCD (iDus-420-OE). Figure S2 shows the normalized UV-vis absorbance spectra of both Ru[bpy]<sub>3</sub><sup>2+</sup> and RuPt in anhydrous acetonitrile. Figures S3a and S3b show the photoluminescence spectra of Ru[bpy]<sub>3</sub><sup>2+</sup> and RuPt in anhydrous acetonitrile at excitation wavelengths ranging from 350 nm to 520 nm.

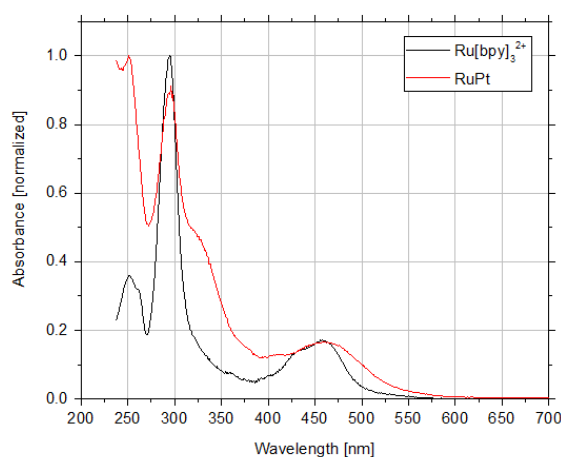


**Figure S2.** Absorbance spectra of Ru[bpy]<sub>3</sub><sup>2+</sup> and RuPt in anhydrous acetonitrile.

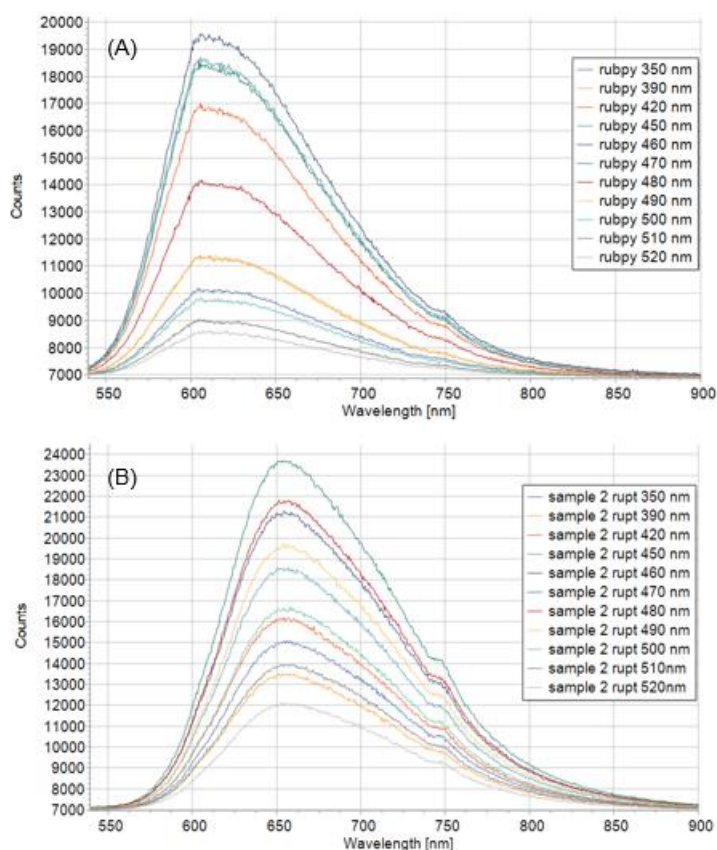


**Figure S3.** Photoluminescence spectra of Ru[bpy<sub>3</sub>]<sup>2+</sup> (A) and RuPt (B) dissolved in anhydrous acetonitrile at various excitation wavelengths.

Table S1 presents the integrated photoluminescence intensity, divided by the fraction of absorbed light  $F_A$  ( $F_A = 1 - 10^{-A}$ , where  $A$  = absorbance in optical density), at that particular excitation wavelength. Assuming that the photoluminescence quantum yield of Ru[bpy<sub>3</sub>]<sup>2+</sup> is independent of excitation wavelength (Kasha's rule), the photoluminescence quantum yield of RuPt may slightly decrease with increasing wavelength, possibly due to an increased population of the T<sub>3</sub> state.

**Table S1.** Overview of integrated photoluminescence intensities, divided by the fraction of absorbed light  $F_A$ , as function of the excitation wavelength.

Excitation wavelength (nm)	Integrated photoluminescence intensity / $F_A$		Ratio RuPt / Ru[bpy <sub>3</sub> ] <sup>2+</sup>
	Ru[bpy <sub>3</sub> ] <sup>2+</sup>	RuPt	
350	3.61E+06	8.04E+06	2.23
390	5.66E+06	1.18E+07	2.09
420	6.36E+06	1.21E+07	1.90
450	5.92E+06	1.13E+07	1.90
460	6.82E+06	1.23E+07	1.80
470	8.31E+06	1.39E+07	1.68
480	8.38E+06	1.49E+07	1.78
490	8.76E+06	1.65E+07	1.88
500	9.23E+06	1.85E+07	2.00
510	9.62E+06	2.13E+07	2.22
520	9.72E+06	2.06E+07	2.13

Values in grey are prone to larger errors because of division in calculation due to scatter at short wavelengths.

#### 4) Differential absorbance spectra at reduction conditions

As the electrochemical reduction of RuPt is not fully reversible, the differential absorbance spectra of its monomeric precursor Ru have been measured at various reduction potentials (Figure S4). The rather similar UV-vis spectra of Ru and RuPt (Figure S5, although the maxima for RuPt are shifted by 11 nm, i.e. ca. 0.07 eV) suggest comparable redox properties. Two differential absorption bands (one at ca. 360 nm and another at ca. 420 nm) are well distinguishable. The band at ca. 360 nm is likely due to the reduced bpy ligand. Analogously, the band around 420 nm is likely due to the reduced tpy ligand.<sup>1</sup> Initially, at -1.07 V neither bpy nor tpy is reduced and no absorption difference compared to the spectrum at 0 V exists. On moving towards more negative potentials (-1.36 V and -1.63 V), predominantly the tpy-band starts appearing, while at -2.00 V the bpy-band has become more intense than the tpy-band. These results indicate that reduction of the bpy ligand requires a more negative potential than for the tpy ligand, indicating that the bpy-based  $\pi^*$  orbital is higher in energy than the tpy-based one.

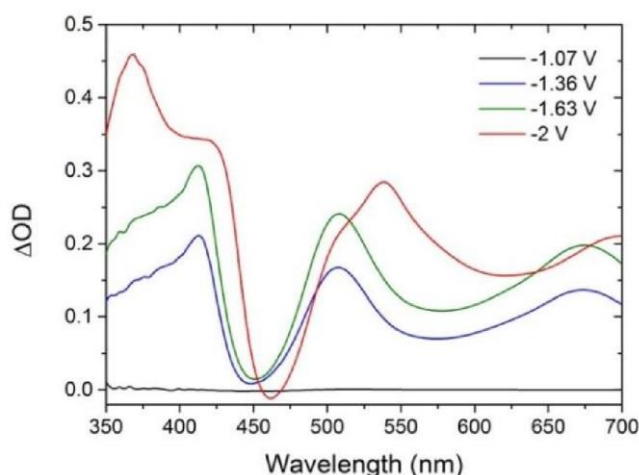


**Figure S4.** Differential absorbance spectra of Ru at various reduction potentials (vs. Ag/AgCl).<sup>1</sup> The spectrum at each potential was recorded after applying the voltage for 10 minutes and corrected for the steady-state absorbance at zero applied bias.

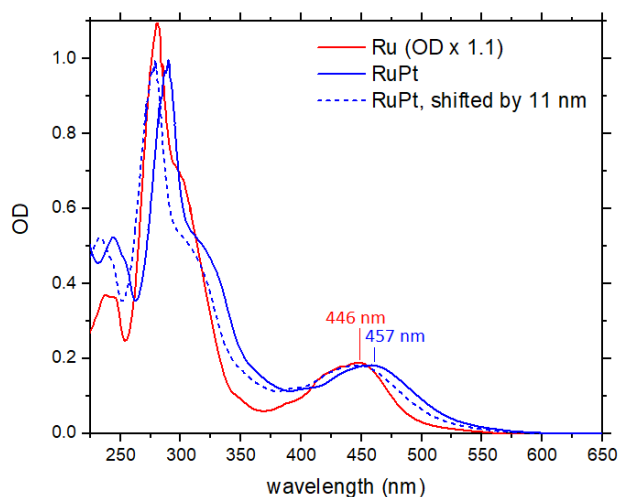


**Figure S5.** Normalized absorbance spectra of Ru and RuPt in anhydrous acetonitrile, including the spectrum of RuPt shifted by 11 nm showing a broadening relative to the spectrum of Ru.

## 5) Transient absorption spectra at various excitation wavelengths

As compared to its monomeric precursor Ru, the UV-vis spectrum of RuPt is redshifted by 11 nm and also broadened (see Figure S5). To gain insight into the nature of optical transitions and the potential involvement of Pt-based transitions<sup>2-3</sup>, Figure S6 compares the transient optical absorption results for RuPt and Ru at various excitation wavelengths. In addition, Time-Dependent Density Functional Theory results are discussed in Section 6.

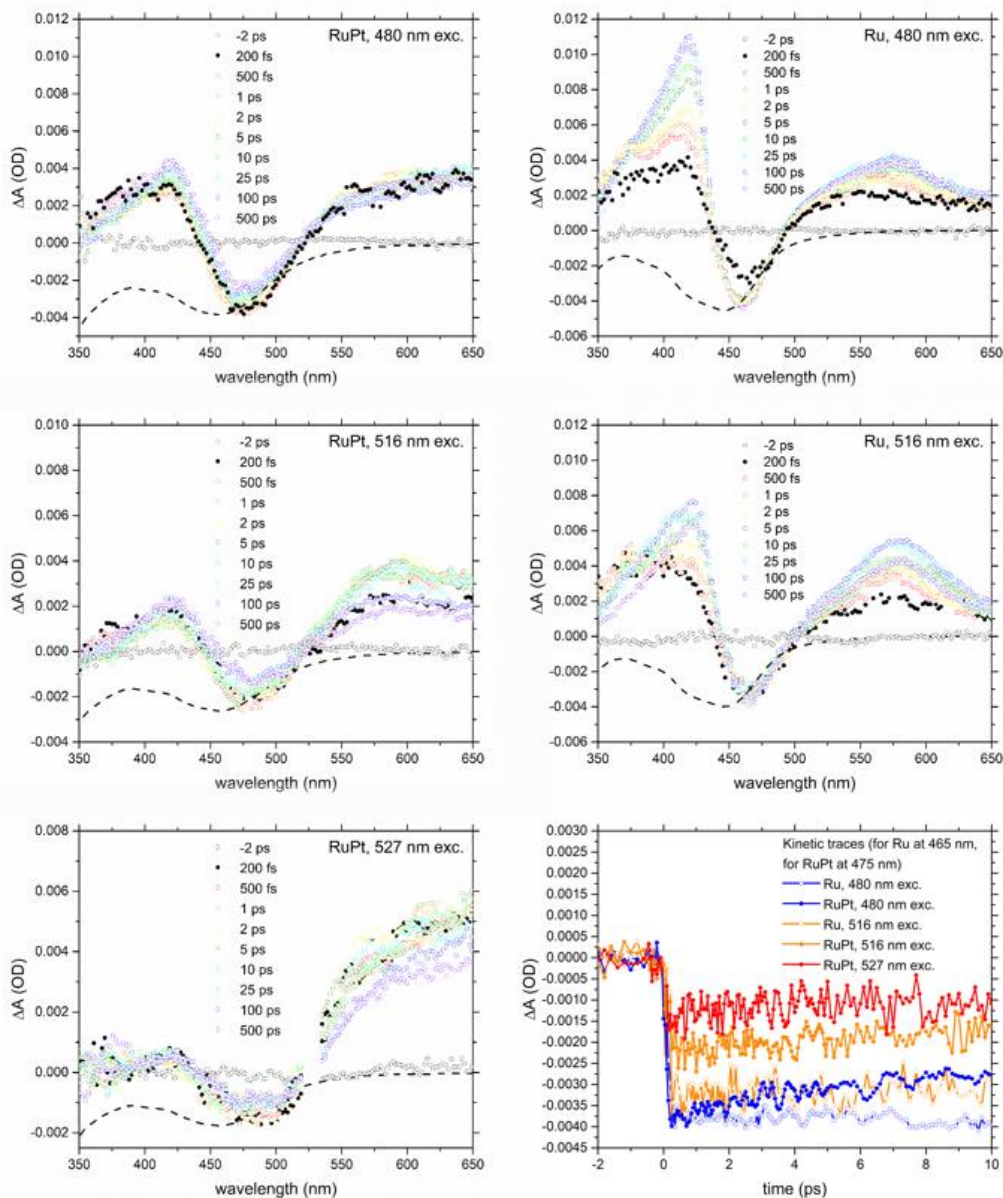


**Figure S6.** Transient absorption spectra of RuPt and Ru at various excitation wavelengths. Also included is the inverted and scaled UV-vis absorption spectrum (dashed line). The panel in the lower right corner shows the kinetic traces at 465 nm (Ru) and 475 nm (RuPt), which signals are due to ground state bleach and possibly excited state absorption.

The origin of the different transient absorption bands and the dynamics is discussed in detail in ref 1. Although the dynamics of Ru and RuPt differ for both complexes a negative signal around 450-500 nm which is slightly redshifted relative to the UV-vis absorption spectrum (included as dashed grey line) is observed.<sup>1</sup> This largest part of this signal is most likely due to ground state bleach, and possibly has some overlap with the positive excited state absorption bands <450 nm and >550 nm. The excited state absorption signals differ

between Ru and RuPt, and also depend on the excitation wavelength. The role of the excitation wavelength in the photodynamics of RuPt can be assigned to a non-equilibrated population of  $^3\text{MLCT}_{\text{bpy}}$ ,  $^3\text{MLCT}_{\text{tpy}}$  and  $T_3$  states<sup>1</sup>, which has motivated the present work. The comparable negative transient absorption bands for Ru and RuPt, both slightly redshifted relative to the UV-vis spectrum, indicates that also for RuPt the Ru-based optical transitions are dominant. This likely applies to all experimental excitation wavelengths shown, as the shape of the negative transient absorption band between 450-500 nm remains nearly constant. The signal develops within the instrumental response time (panel right-below), as expected. A minor contribution of Pt-based optical transitions is however possible.



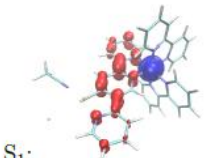
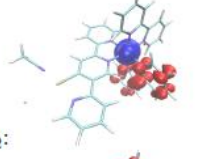
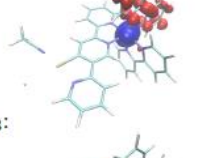
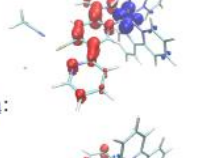
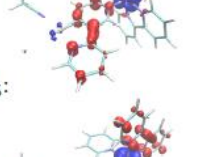
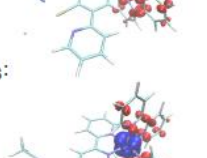

## 6) Time-Dependent Density Functional Theory calculations of optical transitions

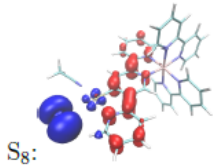
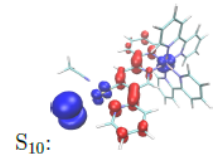
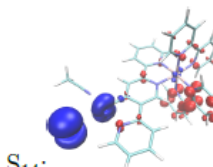
The nature, transition energies and oscillator strengths of the optical transitions in RuPt have been calculated by TD-DFT. Table S2 presents an overview of the results. In orange the most relevant optical transitions, in grey the minor optical transitions that were excited by the 527 nm excitation of the transient x-ray experiments.

### Methods

The electronic absorption spectrum of RuPt has been calculated for the 60 lowest excited states with TD-DFT employing the B3LYP<sup>4-5</sup> functional with the RIJCOSX<sup>6-7</sup> approximation and the COSMO<sup>8-9</sup> implicit solvation model for acetonitrile, using the molecular geometry optimized in Pan et al.<sup>10</sup>. The def2-SVP<sup>11</sup> basis set was used for all atoms, and, additionally, Stuttgart-Dresden quasi-relativistic effective core potentials (MWB) with 28, 46 and 60 electrons were used for Ru, Pt and I respectively. The calculation has been performed with the ORCA 3.0.2 program package.<sup>12</sup>

**Table S2.** Center wavelengths and oscillator strengths of all calculated optical transitions in RuPt, including the nature of the most relevant (orange) and minor (grey) optical transitions in RuPt at 527 nm excitation.

Transition	Wavelength (nm)	f	Type of transition	Orbitals involved
1	581,6	0,0027	Ru-based MLCT	 S <sub>1</sub> :
2	528,8	0,0001	Ru-based MLCT	
3	527,3	0,0004	Ru-based MLCT	
4	528,3	0,0060	Ru-based MLCT	
5	495,2	0,0139	Ru-based MLCT	
6	474,2	0,0003	Ru-based MLCT	
7	463,4	0,0013	Ru-based MLCT	
				 S <sub>2</sub> :
				 S <sub>3</sub> :
				 S <sub>4</sub> :
				 S <sub>5</sub> :
				 S <sub>6</sub> :
				 S <sub>7</sub> :

8	556,4	0,0001	Pt-based MLCT	 S <sub>8</sub> :
9	438,8	0,0082	Ru-based MLCT	
10	481,1	0,0017	Pt-based MLCT	 S <sub>10</sub> :
11	407,7	0,0046		
12	387,1	0,0024		
13	411,2	0,0117		
14	441,7	0,0042	Pt-based MLCT	 S <sub>14</sub> :
15	516,1	0,0000		
16	470,5	0,0001		
17	363	0,0077		
18	360,4	0,0043		
19	357,7	0,0056		
20	505,8	0,0000		
21	351,9	0,0001		
22	344,9	0,0160		
23	342,9	0,0070		
24	344,2	0,0054		
25	342,7	0,0016		
26	369,4	0,0018		
27	336,9	0,0011		
28	332,9	0,0035		
29	330,9	0,0006		
30	329	0,0069		
31	329,4	0,0053		
32	327,4	0,0031		
33	326,4	0,0341		

34	332,2	0,0013		
35	322,3	0,0034		
36	321,7	0,0097		
37	322,3	0,0018		
38	366,6	0,0002		
39	331,2	0,0009		
40	318,6	0,0004		
41	329,4	0,0031		
42	331,2	0,0001		
43	319,3	0,0045		
44	373,1	0,0003		
45	319,5	0,0024		
46	316,7	0,0010		
47	378,7	0,0001		
48	308,6	0,0076		
49	308,1	0,0058		
50	374	0,0000		
51	297,7	0,0034		
52	299,1	0,0071		
53	299	0,0086		
54	299,2	0,0002		
55	322,6	0,0002		
56	309,4	0,0122		
57	305	0,0028		
58	293,5	0,01497		
59	349	0,0002		
60	353,1	0,0001		

## 7) Comparison of white line intensity of modeled and measured XANES

The relative position and intensity of the white line is a sensitive indicator of the oxidation state in Pt complexes. To support the statements made in the paper, two curves were retrieved from the paper from Tsai et al.<sup>13</sup> and are here presented and compared with the modeled curves.

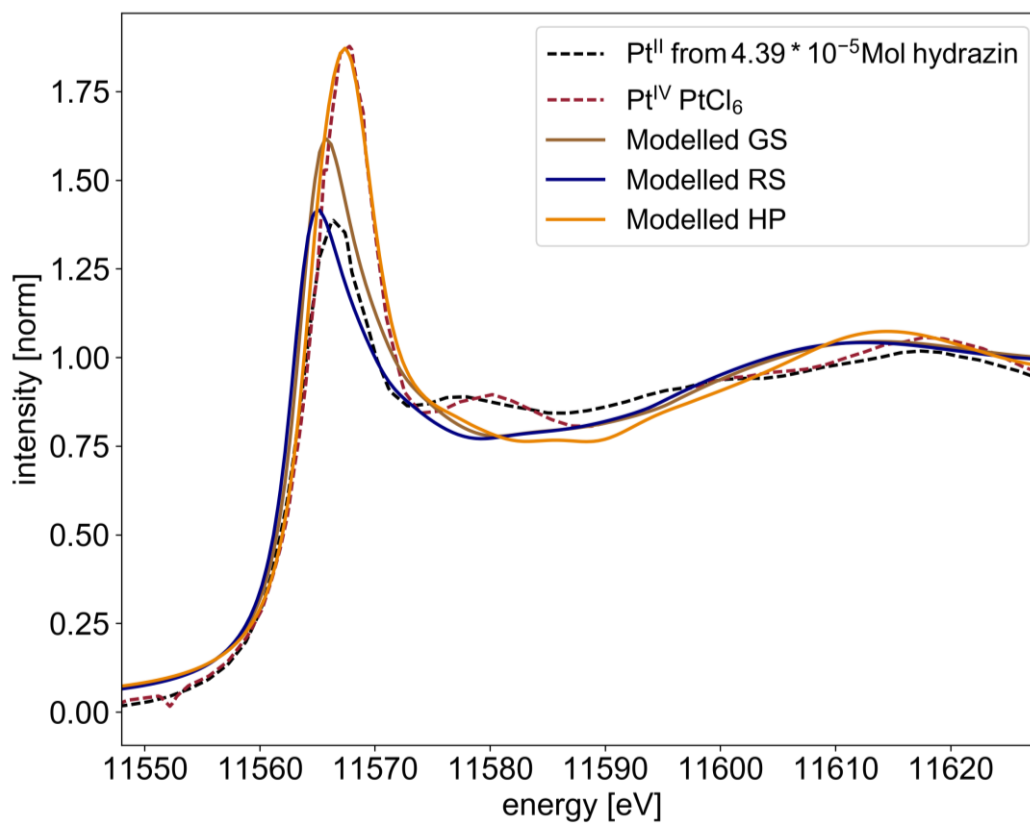


**Figure S7.** Comparison of the modeled XANES with previously published data by Tsai et al.<sup>13</sup>

## References

1. Pan, Q.; Mecozzi, F.; Korterik, J. P.; Vos, J. G.; Browne, W. R.; Huijser, A. The Critical Role Played by the Catalytic Moiety in the Early-Time Photodynamics of Hydrogen Generating Bimetallic Photocatalysts. *ChemPhysChem* **2016**, *17*, 2654-2659.
2. Kobayashi, M.; Masaoka, S.; Sakai, K. Syntheses, Characterization, and Photo-Hydrogen-Evolving Properties of Tris(2,2'-Bipyridine)Ruthenium(II) Derivatives Tethered to an H<sub>2</sub>-Evolving (2-Phenylpyridinato)Platinum(II) Unit. *Molecules* **2010**, *15*, 4908-4923.
3. Kobayashi, M.; Masaoka, S.; Sakai, K. Synthesis, Crystal Structure, Solution and Spectroscopic Properties, and Hydrogen-Evolving Activity of [K(18-Crown-6)][Pt(II)(2-Phenylpyridinato)Cl<sub>2</sub>]. *Photochem. Photobiol. Sci.* **2009**, *8*, 196-203.
4. Lee, C.; Yang, W.; Parr, R. G. Development of the Colle-Salvetti Correlation-Energy Formula into a Functional of the Electron Density. *Phys. Rev. B: Condens. Matter* **1988**, *37*, 785-789.
5. Becke, A. D. Density - Functional Thermochemistry. Iii. The Role of Exact Exchange. *J. Chem. Phys.* **1993**, *98*, 5648-5652.
6. Neese, F.; Hansen, A.; Liakos, D. G. Efficient and Accurate Approximations to the Local Coupled Cluster Singles Doubles Method Using a Truncated Pair Natural Orbital Basis. *J. Chem. Phys.* **2009**, *131*, 064103.
7. Izsák, R.; Neese, F. An Overlap Fitted Chain of Spheres Exchange Method. *J. Chem. Phys.* **2011**, *135*, 144105.
8. Klamt, A.; Schuurmann, G. Cosmo: A New Approach to Dielectric Screening in Solvents with Explicit Expressions for the Screening Energy and Its Gradient. *J. Chem. Soc., Perkin Trans. 2* **1993**, 799-805.
9. Andreas, K. The Cosmo and Cosmo - Rs Solvation Models. *Wiley Interdiscip. Rev. Comput. Mol. Sci.* **2011**, *1*, 699-709.
10. Pan, Q.; Freitag, L.; Kowacs, T.; Falgenhauer, J. C.; Korterik, J. P.; Schlettwein, D.; Browne, W. R.; Pryce, M. T.; Rau, S.; Gonzalez, L., et al. Peripheral Ligands as Electron Storage Reservoirs and Their Role in Enhancement of Photocatalytic Hydrogen Generation. *Chem. Commun.* **2016**, *52*, 9371-9374.
11. Weigend, F.; Ahlrichs, R. Balanced Basis Sets of Split Valence, Triple Zeta Valence and Quadruple Zeta Valence Quality for H to Rn: Design and Assessment of Accuracy. *PCCP* **2005**, *7*, 3297-3305.
12. Frank, N. The Orca Program System. *Wiley Interdiscip. Rev. Comput. Mol. Sci.* **2012**, *2*, 73-78.
13. Tsai, Y. W.; Tseng, Y. L.; Sarma, L. S.; Liu, D. G.; Lee, J. F.; Hwang, B. J. Genesis of Pt Clusters in Reverse Micelles Investigated by in Situ X-Ray Absorption Spectroscopy. *J. Phys. Chem. B* **2004**, *108*, 8148-8152.